Journal of Sound and Vibration (1996) **194**(3), 295–316

OPTIMIZATION OF PASSIVE AND ACTIVE NON-LINEAR VIBRATION MOUNTING SYSTEMS BASED ON VIBRATORY POWER TRANSMISSION

T. J. ROYSTON† AND R. SINGH

Acoustics and Dynamics Laboratory, Department of Mechanical Engineering, The Ohio State University, Columbus, OH 43210-1107, *U.S.A.*

(*Received* 4 *May* 1995, *and in final form* 22 *November* 1995)

While significant non-linear behavior has been observed in many vibration mounting applications, most design studies are typically based on the concept of linear system theory in terms of force or motion transmissibility. In this paper, an improved analytical strategy is presented for the design optimization of complex, active or passive, non-linear mounting systems. This strategy is built upon the computational Galerkin method of weighted residuals, and incorporates order reduction and numerical continuation in an iterative optimization scheme. The overall dynamic characteristics of the mounting system are considered and vibratory power transmission is minimized via adjustment of mount parameters by using both passive and active means. The method is first applied through a computational example case to the optimization of basic passive and active, non-linear isolation configurations. It is found that either active control or intentionally introduced non-linearity can improve the mount's performance; but a combination of both produces the greatest benefit. Next, a novel experimental, active, non-linear isolation system is studied. The effects of non-linearity on vibratory power transmission and active control are assessed via experimental measurements and the enhanced Galerkin method. Results show how harmonic excitation can result in multiharmonic vibratory power transmission. The proposed optimization strategy offers designers some flexibility in utilizing both passive and active means in combination with linear and non-linear components for improved vibration mounts.

1. INTRODUCTION

Enhancements to the traditional linear passive vibration isolation approaches of Den Hartog [1] have been observed in practice to meet the needs for superior vibration mounts. For example, the relatively linear elastomeric engine mount in automobiles is being replaced by a hydro-mechanical mount which has non-linear, frequency and excitation amplitude dependent properties [2]. Improved vibration isolation has also been attempted via adaptive or actively controlled mechanisms. Again, in automotive applications, adaptive systems provide more control over the mode of operation of the mount, whether high stiffness/damping or low stiffness/damping properties are desired [2–4]. Active vibration isolation systems, which essentially use a secondary energy source or force, have been employed in automotive, aircraft, and rotorcraft applications as well [4–6]. Despite these trends, few research investigators have considered non-linear effects in passive, adaptive, or active vibration mount design analyses. Since in many

† Present address: Department of Mechanical Engineering, The University of Illinois at Chicago, Chicago, IL 60607-7022, USA.

0022–460X/96/280295 + 22 $18.00/0

practical situations, non-linear characteristics, whether intentional or unintentional, play a significant role in influencing system performance, a need exists for a more fundamental study. It is the main focus of this article. However, only the steady state vibration isolation problem is considered from the vibratory power transmission viewpoint.

2. LITERATURE REVIEW

Several recent investigators have re-examined the classical linear passive vibration isolation or absorption strategy of Den Hartog through the use of non-linear components [7–13]. While most studies have considered non-linearity in the context of the tuned absorber configuration [7–11], a few have applied it to the zero-degree-of-freedom (d.o.f.) isolator configuration, i.e. a massless spring-damper element [12–13]. Many of these studies have found that non-linearity in stiffness can lead to improved mount performance. In particular, improvements have been reported in studies using non-linear stiffness elements in either the primary spring [8, 9, 11, 12] and/or the secondary spring [7–11]. Whether a hardening [8] or softening [7, 12] stiffness (or both [9–11]) results in ''perceived superior'' performance has depended on the specific system properties and the criterion used to assess performance. In these studies, only the harmonic response to harmonic excitation is assumed and typical performance criteria are based on either motion or force transmissibilities. In some other studies of comparable systems, the steady state response at harmonics other than the fundamental has been found to be significant [14–16]. Omission of such spectral contents may lead to an incorrect assessment of mount performance.

In many research articles, a fairly simplified support base, either fixed or a single d.o.f. system is typically assumed. However, practical systems, often consisting of compliant structures, may demand a more realistic and complex multiple d.o.f. mathematical treatment for both supporting bases and mounted components [17]. Relative impedances between the mounted assembly and the support structure, which may vary significantly over a wide frequency range due to numerous system resonances, may render use of a few selected displacement or force variables a somewhat poor method of assessing mount performance. This situation is exacerbated in non-linear systems, where impedances can be amplitude dependent as well, and the dynamic response may have a wider spectral content, even for harmonic excitation. Vibrational power transmission through the mount into the supporting structure, which depends upon both force and motion vectors, is probably a more accurate performance descriptor [18, 19]. No previous study to the best of the authors' knowledge has analyzed vibratory power transmission in a non-linear mount or isolator.

Improvement via active control strategies has also been undertaken by many investigators [20–23]. For instance, Jenkins *et al*. [20] obtained better performance and stability when an active force component was placed in parallel with conventional passive springs and dampers. In their detailed theoretical and experimental study, minimization of the acceleration at multiple locations on a flexible supporting structure was used as the performance index. This investigation highlighted the adverse impact that the finite size and resulting non-collocation of parallel active and passive isolation elements have on performance. Scribner *et al*. [21] studied how a multi-resonant support structure can adversely affect the mounting system performance. Collocated passive and active mount components stacked in series were used with minimization of transmitted force to the supporting structure as the performance criterion. This criterion was favored over a motion-based one because it offered better two-way vibration isolation, meaning that vibration is not transmitted back to the machine from the support structure. Pan and

Hansen [22] and Pan *et al*. [23] considered the use of vibratory power transmission through a collocated active/passive mount as a performance index, with the claim that it is a more direct measure of the vibratory energy flow into a flexible support structure. They also indicated the need to account for multi-dimensional power transmission through the mount, involving both rotational and translational degrees-of-freedom.

In all of the publications cited and in numerous other studies, the linear system theory is invariably assumed. Gaining a clear understanding of active control applied to non-linear mounting systems remains an immense technical challenge that will undoubtedly drive much future research. At this point however, a more important intermediate step is to identify some issues introduced by the presence of significant non-linear interactions in the passive component of the active/passive mount. Two questions which still remain unanswered are: (a) what is the role of non-linear dynamic interactions on conventional active control approaches, and (b) can non-linear effects and active control be concurrently employed to improve the performance of a vibration mount? An attempt will be made in this article to provide some preliminary answers.

3. PROBLEM FORMULATION

Given current enhancements and trends in practical vibration mount design, an analytical framework is needed that can: (1) capably handle non-linearity, both as a system property and as an optimization parameter; (2) use vibratory power flow for performance assessment instead of motion or force transmissibility-type descriptors by themselves; and (3) consider active control approaches in the context of non-linear system behavior. A fundamental barrier to undertaking such a comprehensive approach is obviously the degree of difficulty encountered when analyzing non-linear dynamics in an extensive, multi-dimensional system. A recent article by the authors [15] has provided an efficient semi-analytical framework for the analysis of such systems. A companion article [16] has demonstrated its usefulness in the study of a novel, experimental system possessing a localized non-linearity and many degrees-of-freedom. In the current article, this framework is extended further as the foundation for a mount optimization strategy incorporating nonlinear effects, vibratory power flow calculations, and active control concepts per discussion in Section 2.

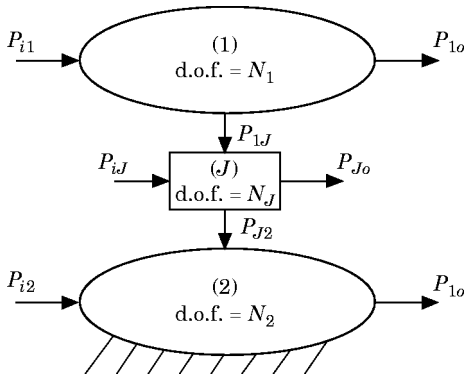

Figure 1. Vibration mounting system from the vibratory power flow perspective. Here, (1) refers to the mounted machine or equipment element, (2) refers to the flexible supporting structure, and (J) refers to the non-linear mount. Vibratory power flow P into (i) and out of (o) the system and between its elements (1, 2 and J) is denoted by arrows.

Figure 1 illustrates conceptually a vibration mounting system. A machine or equipment element (1) is mounted on a supporting structure (2) through a non-linear mount (J). The mounted machinery may be under both dynamic (in this study, periodic) and static (time-invariant) excitation due to forces associated with machine operation and weight, respectively. The dynamic excitation component results in vibrational power flow into the subsystem, P_{i1}. Vibrational energy of the subsystem is either dissipated, P_{1o}, or transmitted through the non-linear mount, P_{1J}. Similarly, in the non-linear mount, vibrational energy again may be dissipated, P_{Jo}, or transmitted to the supporting structure, P_{J2}. If an active mount is present, its vibrational energy must also be added, P_{iJ}. In the supporting structure, vibrational energy is eventually dissipated, P_{2o}. Disturbances to the supporting structure itself, such as the effect of variation in the road profile on the automotive chassis, may result in vibrational energy input directly to the supporting structure, P_{i2}, some of which may be transmitted through the mount and into the mounted machine or equipment element. Hence, P_{1J} and P_{J2}, as defined, may be negative. While the localized non-linearity of Figure 1 in the mount may be confined to only a few degrees-of-freedom, N_J, the entire system must be considered for dynamic analysis, including the mounted structure of dimension N_1, and the supporting structure of dimension N_2.

Specific objectives of this study are to: (1) Formulate a theoretical framework for the optimization of the system proposed in Figure 1, a multi-degree-of-freedom vibration mounting system which considers (a) mount non-linearity, (b) active control, and (c) vibratory power transmission; (2) develop a computational strategy for efficient implementation of the optimization procedure; and (3) apply the framework and strategy to two different example case systems. For the first example case, optimization of a mounting system using different combinations of passive-linear, passive-non-linear, and active control parameters is computationally explored. For the second example case, the nature of vibratory power flow in a multi-dimensional, active or passive, non-linear mounting system is experimentally investigated. The effect of system non-linearity on the conventional feedforward active vibration control strategy is briefly explored.

4. NON-LINEAR OPTIMIZATION STRATEGY

Consider a periodic excitation of the system in Figure 1 with fundamental frequency ω. Assuming non-chaotic behavior, the system will respond periodically with subharmonics and superharmonics of the excitation. Let m and n respectively denote the highest order non-negligible subharmonic and superharmonic in the response, which consequently has a fundamental period $m(2\pi/\omega)$. By selecting a suitable non-dimensional time variable $\tau = \omega t/m$, any dynamic displacement (q) and force (F_q) response variables of the entire system can be expressed in the following series forms; also refer to Appendix A for the identification of symbols:

$$\mathrm{q}^{mn}(\tau) = a_0^q + \sum_{k=1}^{mn} a_{2k-1}^q \sin(k\tau) + a_{2k}^q \cos(k\tau), \tag{1a}$$

$$\mathrm{F}_q^{mn}(\tau) = a_0^{F_q} + \sum_{k=1}^{mn} a_{2k}^{F_q} - 1 \sin(k\tau) + a_{2k}^{F_q} \cos(k\tau). \tag{1b}$$

From equations (1a, b), expressions for steady state vibratory power transmission throughout the system can be formulated. For example, assume that the mount is connected to the support structure by an N_y dimensional displacement vector $\mathbf{y}$ which could

contain translational and rotational degrees-of-freedom. Vibratory power flow from the mount into the support structure P_{J2} would be expressed as

$$P_{J2}(\omega) = \sum_{s=1}^{N_v} \sum_{k=1}^{mn} \frac{k\omega}{2m} [-a_{2k-1}^{F_{js}} a_{2k}^{v_s} + a_{2k}^{F_{js}} a_{2k-1}^{v_s}]. \tag{2}$$

In general the goal of a vibration isolator is to minimize some scalar cost function J_o that is somehow related to vibratory power transmission. In Figure 1, J_o may be a function of P_{J2}, the vibratory power transmission into the supporting structure. In the context of a design optimization problem, P_{J2} is a scalar function of $\mathbf{\Gamma}$, the N_Γ dimensional vector of mount parameters which may be modified. Consequently, $J_o \equiv J_o[P_{J2}(\mathbf{\Gamma})]$. An optimization problem with a cost function based on P_{J2} for harmonic excitation over a range of frequencies (say ω_{low} to ω_{high}) at a particular excitation level could be formulated as

$$\underset{\Gamma}{\text{minimize}}\, J_o[P_{J2}(\mathbf{\Gamma})] = \int_{\omega_{low}}^{\omega_{high}} P_{J2}(\mathbf{\Gamma}, \omega)\, \mathrm{d}\omega \approx \sum_{l=0}^{N_l} P_{J2}(\mathbf{\Gamma}, \omega_l), \tag{3a}$$

where

$$\omega_l = (l/N_l)(\omega_{high} - \omega_{low}) + \omega_{low}. \tag{3b}$$

Hence, the integral of the vibratory power flow into the supporting structure between frequencies ω_{low} and ω_{high} is approximated with a finite summation. Note that in those situations where multiple stable solutions exist at a given frequency, the cost function is ambiguous. It will then be necessary to choose a particular solution or use an averaged value.

For the optimization problem, $J_o(\mathbf{\Gamma})$ is expected to be a highly non-linear function defined over the N_Γ dimensional space spanned by values of $\mathbf{\Gamma}$. In this space $\mathbf{Q}$ of allowable values of $\mathbf{\Gamma}$, $J_o(\mathbf{\Gamma})$ may have many local minima. Evaluation of $J_o(\mathbf{\Gamma})$ over all of $\mathbf{Q}$ may be computationally prohibitive or impossible. One alternate iterative approach is to first minimize $J_o(\mathbf{\Gamma})$ on the subplane in $\mathbf{Q}$ spanned by the linear mount parameters Γ_L, which is more easily accomplished since, on this plane, linear techniques for the solution of J_o are applicable. Then, starting from this solution point in the subspace of $\mathbf{Q}$, additional dimensions of $\mathbf{Q}$ can be included in an iterative, gradient-based optimization process. Consequently, the process will converge to a local minimum point $\mathbf{\Gamma}^{\mathbf{opt}}$ in the vicinity of the optimal linear mount configuration. This point may or may not be globally minimal, but it may be practically feasible since it was reached from a more conventional linear solution. Other starting points and sequences for adding additional dimensions in $\mathbf{Q}$ may be chosen based on *a priori* knowledge of an actual physical device or even intuition.

The proposed optimization strategy is summarized in block diagram form in Figure 2. In a companion article [15], an efficient non-linear solution method for a system similar to Figure 1 was developed and verified via direct time digital numerical integration and analog computer simulation. The method is based on the Galerkin procedure and employs order reduction to reduce the number of degrees-of-freedom to be solved using the iterative strategy, and continuation to aid in parametric studies. This method is used as a subroutine to solve for the coefficient values, a_k^q and $a_k^{F_q}$, of equations (1a, b) in the optimization code. Its application in this context is briefly reviewed here to enhance the clarity of presentation.

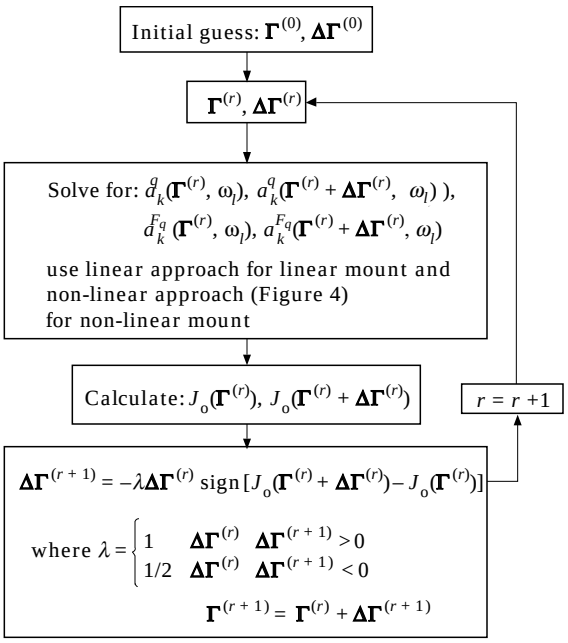

Figure 2. Vibratory-power-based optimization procedure for non-linear mounts.

The system of Figure 1 can be divided into two sections, shown in Figure 3. Section (A) contains N_x degrees-of-freedom with non-linearities defined in the time domain and/or driven by external forces. For this section, the equations of motion can be expressed as

$$\mathbf{d}^x(\tau) \equiv \mathbf{X}[\mathbf{x}(\tau), \mathbf{y}(\tau), \dot{\mathbf{x}}(\tau), \dot{\mathbf{y}}(\tau), \tau] - \ddot{\mathbf{x}}(\tau) = \mathbf{0}, \quad \mathbf{d}^x \equiv [d^{x_1}, d^{x_2}, \ldots, d^{x_{N_x}}]^T. \tag{4}$$

Here $\mathbf{x}$ refers to the vector of displacement variables in Section (A) and $\mathbf{y}$ refers to the N_y-degree-of-freedom vector of displacement variables describing the interfacial connection of Section (B) to Section (A).

Section (B) contains all of the remaining linear degrees-of-freedom as well as the degrees-of-freedom with non-linearities defined in the frequency domain, N_w. This section can be analyzed completely in the frequency domain using linear algebraic methods.

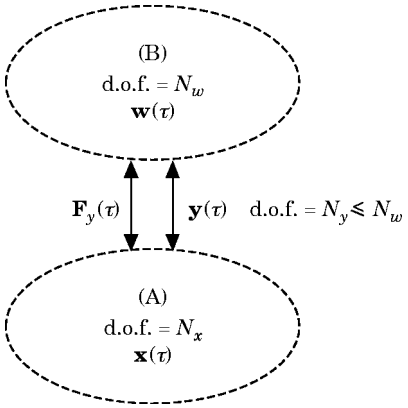

Figure 3. Enhanced Galerkin technique based on the subsystem structuring concept. Here, N_y denotes the dimension of the force/displacement connection between Sections (A) and (B).

Displacement of Section (B) at the connection point to Section (A), as indicated above, is described by the vector $\mathbf{y}(\tau)$ which is a linear mapping of $\mathbf{w}(\tau)$. Likewise, the force vector at this connection point is described by an N_y-degree-of-freedom vector $\mathbf{F}_y(\tau)$. Hence, for Section (B), a frequency dependent transfer function may be defined as follows where $\sim$ denotes a complex number and ω' is an arbitrary response frequency:

$$\tilde{\mathbf{T}}_y(\omega') \equiv \tilde{\mathbf{y}}/\tilde{\mathbf{F}}_y(\omega'). \tag{5}$$

Now, the mnth approximate solution to the problem will have the form

$$\mathbf{x^{ma}}(\tau) = \mathbf{a_0^x} + \sum_{k=1}^{mn} \mathbf{a_{2k-1}^x} \sin(k\tau) + \mathbf{a_{2k}^x} \cos(k\tau), \quad \mathbf{a_k^x} \equiv [a_k^{x_1}, a_k^{x_2}, \ldots, a_k^{x_{N_x}}]^T, \tag{6a}$$

$$\mathbf{y^{mn}}(\tau) = \mathbf{a_0^y} + \sum_{k=1}^{mn} \mathbf{a_{2k-1}^y} \sin(k\tau) + \mathbf{a_{tk}^y} \cos(k\tau), \quad \mathbf{a_k^y} \equiv [a_k^{y_1}, a_k^{y_2}, \ldots, a_k^{y_{N_y}}]^T, \tag{6b}$$

By substituting expressions (6a, b) into equation (4) and numerically calculating the Fourier coefficients of $\mathrm{d}^{x^{mn}}(\tau)$, one obtains the following $(4mn + 1) \times (N_x)$ non-linear algebraic determining equations for finding the values of the coefficients:

$$\boldsymbol{\alpha}^{\mathbf{x}} \equiv [\mathbf{a_0^x} \quad \mathbf{a_1^x} \quad \cdots \quad \mathbf{a_{4mn}^x}], \quad \boldsymbol{\alpha}^{\mathbf{y}} \equiv [\mathbf{a_0^y} \quad \mathbf{a_1^y} \quad \cdots \quad \mathbf{a_{4mn}^y}],$$

$$\mathbf{D_j^{xmn}}(\boldsymbol{\alpha}) \equiv \mathscr{F}_j[\mathbf{d^{xmn}}(\tau)] = \mathbf{0}, \quad j = 0, \ldots, 4nm,$$

where

$$\boldsymbol{\alpha} \equiv [\boldsymbol{\alpha}^{\mathbf{x}} \quad \boldsymbol{\alpha}^{\mathbf{w}}]^{\mathbf{T}}, \mathscr{F}_0[\mathrm{d}(\tau) \equiv \frac{1}{2P} \sum_{p=1}^{2P} \mathrm{d}(\tau_p), \mathscr{F}_{2k-1}[\mathrm{d}(\tau)] \equiv \frac{1}{P} \sum_{p=1}^{2P} \mathrm{d}(\tau_p) \sin(k\tau_p),$$

$$\mathscr{F}_{2k}[\mathrm{d}(\tau)] \equiv \frac{1}{P} \sum_{p=1}^{2P} \mathrm{d}(\tau_p) \cos(k\tau_p), \quad k = 1, \ldots, 2nm,$$

and

$$\tau_p = (2p - 1)\pi/(2P), \; P \geqslant 2nm, \; p = 1, \ldots, P. \tag{7}$$

The remaining $(4mn + 1) \times (N_y)$ determining equations needed take the form

$$\mathbf{D_0^{ymn}}(\boldsymbol{\alpha}) \equiv \sum_{s=1}^{N_y} \{\mathrm{Re}[\tilde{\mathbf{T}}_{\mathbf{y}}^{\mathbf{r,s}}(0)] a_0^{F_{y_s}}\} - a_0^{y_r} = 0, \tag{8a}$$

$$D_{2k-1}^{ym}(\boldsymbol{\alpha}) \equiv \sum_{s=1}^{N_y} \left\{ \mathrm{Re}\left[\tilde{\mathrm{T}}_y^{r,s}\left(\frac{k\omega}{m}\right)\right] a_{2k-1}^{F_{y_s}} + \mathrm{Im}\left[\tilde{\mathrm{T}}_y^{r,s}\left(\frac{k\omega}{m}\right)\right] a_{2k}^{F_{y_s}} \right\} - a_{2k-1}^{y_y} = 0, \tag{8b}$$

$$D_{2k}^{ymn}(\boldsymbol{\alpha}) \equiv \sum_{s=1}^{N_y} \left\{ \mathrm{Re}\left[\tilde{\mathrm{T}}_y^{r,s}\left(\frac{k\omega}{m}\right)\right] a_{2k}^{F_{y_s}} - \mathrm{Im}\left[\tilde{\mathrm{T}}_y^{r,s}\left(\frac{k\omega}{m}\right)\right] a_{2k-1}^{F_{y_s}} \right\} - a_{2k}^{y_y} = 0, \tag{8c}$$

where

$$r = 1, \ldots, N_y, \; k = 1, \ldots, 2mn \quad \text{and} \quad a_j^{F_{y_s}} \equiv \mathscr{F}_j[F_{y_s}^{mn}(\tau)], \quad j = 0, \ldots, 4mn.$$

Consequently, using this order reduction technique, the number of coupled non-linear algebraic equations to be solved iteratively remains fixed at $N = (N_y + N_z) \times (4nm + 1)$

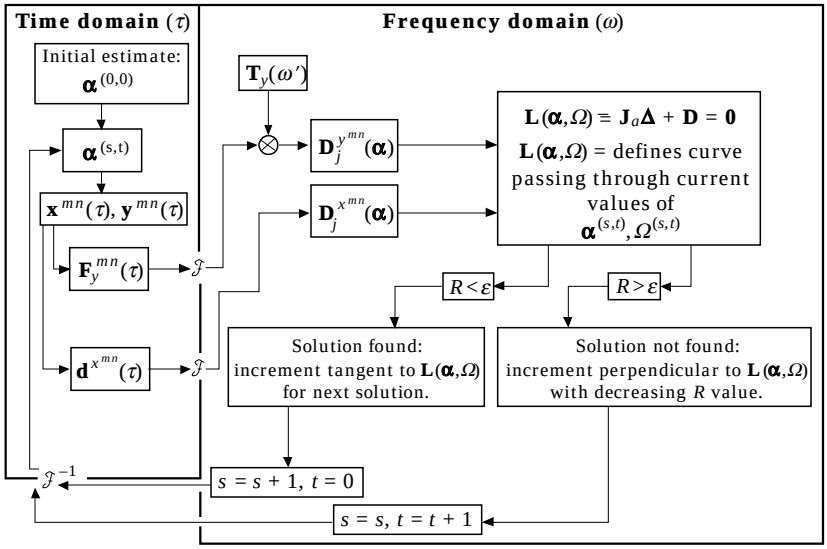

Figure 4. Conceptual algorithm of the enhanced Galerkin method.

regardless of the number of degrees-of-freedom N_w in Section (B). Once the non-linear solution is obtained, the response of any degree-of-freedom in Section (B) is quickly found by using linear algebra.

The Galerkin method essentially employs an iterative method to solve the coupled non-linear algebraic equations, minimizing the sum of the squares of the determining equations in the frequency domain:

$$R = \sum_{j=0}^{4nm} \left\{ \sum_{s=1}^{N_x} |D_j^{x_s^{mn}}|^2 + \sum_{s=1}^{N_y} |D_j^{y_s^{mn}}|^2 \right\}. \tag{9}$$

Note that while only $nm + 1$ frequencies (including static) are used in the approximate solutions of $\mathbf{x}$ or $\mathbf{y}$, $2nm + 1$ frequencies are used in the calculation of R. Hence, the ensuing truncation error is accounted for as well. The QR decomposition in a Newton-Raphson based continuation strategy is used to solve the equations over a range of any system or excitation parameter Ω which could be chosen as mount stiffness or excitation frequency ω. Calculation of the augmented Jacobian $\mathbf{J}_a \equiv [\partial\mathbf{D}/\partial\alpha \ \partial\mathbf{D}/\partial\Omega]$ of the determining equations in the frequency domain with respect to the unknown Fourier coefficients $\boldsymbol{\alpha}$ and Ω, is required where $\mathbf{D} \equiv [\mathbf{D}^{x^T} \ \mathbf{D}^{y^T}]^T$. Further details of the method can be found in reference [15]. The procedure is also summarized in Figure 4 in a block diagram form. Note that after using the approach of Figure 4 to find a curve of solutions for $\boldsymbol{\Gamma}$ and $\omega_{low} < \omega < \omega_{high}$, the following adaptation can be implemented to iterate from these solutions to other solutions in the neighborhood for $\boldsymbol{\Gamma}$ and $\boldsymbol{\Gamma} + \Delta\boldsymbol{\Gamma}$ at the specific values of ω_1 required for a consistent calculation of J_o:

$$\mathbf{L}(\boldsymbol{\alpha}) \equiv (\partial\mathbf{D}/\partial\boldsymbol{\alpha})\Delta\boldsymbol{\alpha} + \mathbf{D} = \mathbf{0}. \tag{10}$$

Essentially, a standard Newton-Raphson approach is used in place of the continuation approach based on QR decomposition.

5. EXAMPLE CASE I: COMPUTATIONAL STUDY OF A NON-LINEAR VIBRATION ISOLATOR

5.1. ANALYTICAL FORMULATION

Benchmark computational studies of a generic vibration isolation system are first considered to assess the capability of the proposed optimization strategy. The system shown in Figure 5 is chosen because, while it is relatively simple from the analytical viewpoint, it still contains the following ingredients found in many practical systems: (i) a flexible resonant, multi-degree-of-freedom base (2), (ii) parallel linear-passive, non-linear passive, and active mount design parameters (J), and (iii) a periodic excitation source.

For the simply supported beam, the dynamics can be described by the following Euler's beam equation [24]:

$$\rho A\ddot{u}(s, t) + EI\frac{\partial^4 u}{\partial s^4}(s, t) = F_y(t)\delta(s - s_b). \tag{11}$$

Here, ρ, A, E, I, δ and s_b refer to the beam material density, cross-sectional area, Young's modulus, moment of inertia, the Dirac delta function, and the axial position of the mount connection to the beam, respectively. Modal decomposition for the simply supported beam of length l_s is performed to obtain N_w coupled, ordinary differential equations. At a given frequency ω' one has

$$F_y(t) = \tilde{F}_y\, e^{i\omega' t}, \quad u(s, t) = \sum_{j=1}^{N_w} \tilde{u}_j \sin(j\pi s/l_s)\, e^{i\omega' t}, \tag{12a, b}$$

which yield

$$m_b \boldsymbol{\Psi}^{-1}(\omega')\begin{bmatrix}\tilde{u}_1\\ \vdots\\ \tilde{u}_{N_w}\end{bmatrix} = \mathbf{H}^T\tilde{F}_y, \quad \boldsymbol{\Psi} \equiv \begin{bmatrix}\tilde{\boldsymbol{\Psi}}_1 & \cdots & 0\\ \vdots & \ddots & \vdots\\ 0 & \cdots & \tilde{\boldsymbol{\Psi}}_{N_w}\end{bmatrix},$$

$$\tilde{\boldsymbol{\Psi}}_j \equiv 1/(\omega_j^2 - \omega^2 + i2\zeta_j\omega\omega_j), \quad \mathbf{H} \equiv [\sin(\pi s_b/l_s) \quad \cdots \quad \sin(N_w\pi s_b/l_s)],$$

and

$$\omega_j \equiv \sqrt{EI/\rho A}\,(j\pi/l_s)^2, \quad m_b \equiv \rho A l_s/2, \quad j = 1, \ldots, N_w. \tag{13}$$

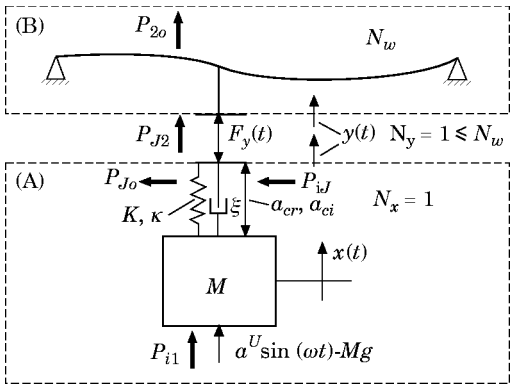

Figure 5. Example Case I. Computational study of an active, non-linear mounting system.

TABLE 1

Summary of numerical example (Case I) results

a: System parameter values which are constant

$\zeta_j = 0{\cdot}005$ for $j = 1, \ldots, N_w$ $\quad N_w = 6$ $\quad s_b/l_s = 3/8$ $\quad \mu = 7{\cdot}4349$ $\quad a^U = 2{\cdot}294$ $\quad m = 1, n = 15$

b: Design parameter values for the optimal mount*

Subcase	K/μ	ξ	$a_{rc} \times 10^6$	$a_{ic} \times 10^6$	κ	$J_0[P_{J2}] \times 10^4$	$J_0[F_{TR}]\%$
a	**1**	0·01	0	0	0	**10·76**	**12·63**
b	**1**	**0·1687**	0	0	0	**2·041**	7·880
–	**1**	**0·1345**	0	0	0	2·078	**7·819**
c	**1**	0·01	**8·8037**	**0·6773**	0	**5·411**	9·031
–	**1**	0·01	**7·0649**	**0·6694**	0	5·618	**8·679**
d	**1**	**0·3128**	**6·3965**	**17·064**	0	**0·941**	4·270
–	**1**	**0·2371**	**4·0343**	**11·745**	0	1·0071	**4·171**
e	**1·2632**	**0·1044**	0	0	**−0·2084**	**1·387**	5·550
f	**1·2088**	**0·1679**	**4·0147**	**−9·5349**	**−0·1727**	**0·696**	3·315

*Bold type indicates an optimized value.

Note that a proportional viscous damping ratio ζ_j has been assumed. From equations (11–13), it follows that if

$$\tilde{y}(\omega) = \mathbf{H}\begin{bmatrix} \tilde{u}_1 \\ \vdots \\ \tilde{u}_{N_b} \end{bmatrix}, \quad \text{then} \quad \tilde{T}_y(\omega') \equiv \frac{\tilde{y}}{\tilde{F}_y}(\omega') = \frac{1}{m_b}\mathbf{H}\Phi(\omega')\mathbf{H}^{\mathbf{T}}. \tag{14a, b}$$

Here, note that $N_y = 1$ regardless of the number of beam modes (N_w) considered.

In order to reduce the number of system variables, equations are expressed in non-dimensional form with displacement variables q replaced with $q(\omega_b^2/g)$, force variables F_q replaced with $F_q/m_b g$, excitation frequency ω replaced with ω/ω_b and response frequency variable ω' replaced by ω'/ω_b. Here, ω_b and g refer to the natural frequency of the first beam mode ($\omega_b = \omega_1$) and the gravitational constant, respectively. Thus equation (14b) as can be rewritten:

$$\tilde{T}_y(\omega') = \mathbf{H}\begin{bmatrix} 1/(1 - \omega'^2 + \mathrm{i}2\zeta_1\omega') & \cdots & 0 \\ \vdots & \ddots & \vdots \\ 0 & \cdots & 1/(N_w^4 - \omega'^2 + \mathrm{i}2\zeta_{N_w}\omega' N_w^2) \end{bmatrix}\mathbf{H}^{\mathbf{T}}, \tag{15}$$

For the example case parameters of Table 1, the magnitude of this expression is shown in Figure 6 for the sake of illustration. Thus, at a given response frequency ω', Section (B) can be completely characterized by the following system parameters: $\zeta_j, j = 1, \ldots, N_w$, and s_b/l_s.

The single-degree-of-freedom non-linear equation for the mount and mounted rigid body, Section (A), may be expressed in the dimensionless form as follows:

$$(m/\mu\omega^2)(a^U \sin(m\tau) - \mu - F_y(\tau)) - \ddot{x}(\tau) = 0, \quad \mu \equiv M/m_b, \tag{16a}$$

$$F_y(\tau) = K[1 + \kappa(x(\tau) - y(\tau))^2](x(\tau) - y(\tau)) + 2\xi\sqrt{\mu K}(\omega/m)(\dot{x}(\tau) - \dot{y}(\tau)) + F_{AC}(\tau), \tag{16b}$$

$$F_{AC}(\tau) = a_{rc} \sin(m\tau) + a_{ic} \cos(m\tau). \tag{16c}$$

Thus, the vector of design parameters for the mount can be written as $\mathbf{\Gamma} \equiv [K \ \xi \ a_{rc} \ a_{ic} \ \kappa]$. The first two terms are linear passive parameters, the next two are active parameters and the last term is a non-linear passive parameter. It should be noted that in this study

a somewhat simplistic approach to active control has been taken. The control force frequency is commensurate with the excitation frequency and the control force amplitude and phase are assumed to be invariant to changes in excitation frequency.

An optimization criterion is now formulated based on vibratory power flow as given by equation (3) with $\omega_{low} = 0{\cdot}75\omega_b$, and $\omega_{high} = 10\omega_b$. An alternate criterion based on the conventional "harmonic" force transmissibility descriptor may also be considered, $J_o[F_{TR}(\mathbf{\Gamma})]$. For this, $P_{J2}(\mathbf{\Gamma}, \omega, a^U)$ is replaced in equation (3) with the root-mean-square of the harmonically transmitted force relative to the excitation force:

$$F_{TR}(\mathbf{\Gamma}, \omega) = \sqrt{(a_m^{F_y})^2/(a^U)^2}. \tag{17}$$

Stability issues limit the applicable range of κ. If κ is too large relative to K, the system may enter a chaotic regime, and the underlying assumptions used in the computational solution strategy would be violated. In addition, an arbitrarily defined maximum allowable static deflection (given by subscript *st*) places a lower limit on K and κ expressed in the following inequality:

$$|x_{st} - y_{st}| \leqslant 1 \Rightarrow K[1 + \kappa] \geqslant \mu. \tag{18}$$

5.2. RESULTS

Several optimal subsets of $\mathbf{\Gamma}$ are found, corresponding to linear passive, linear active, non-linear passive, and non-linear active configurations and these results are summarized in Table 1. First, consider the linear passive mount. The cost function $J_o[P_{J2}]$ as a function of K and ξ is shown in Figure 7. While an optimal linear viscous damping value exists within the boundaries placed on ξ, clearly the best linear stiffness value K is the lowest allowable value based on static deflection considerations. From Table 1 it is seen that the optimal mount configuration based on the force transmissibility criterion is similar for this case. In Figure 8, vibratory power transmission $P_{J2}(\omega)$ as a function of excitation frequency ω is shown for the optimal values of K and ξ as well as for the case with non-optimal damping. This figure shows that the selected frequency range for the optimization criteria covers the second, third and fourth system resonances which are associated with out-of-phase motion between the rigid mass and the first three modes of the simply supported beam.

This approach is further expanded to include the active mount force $F_{AC}(\tau)$ so that a_{rc} and a_{ic} are now added to the set of design parameters. Computational studies show again

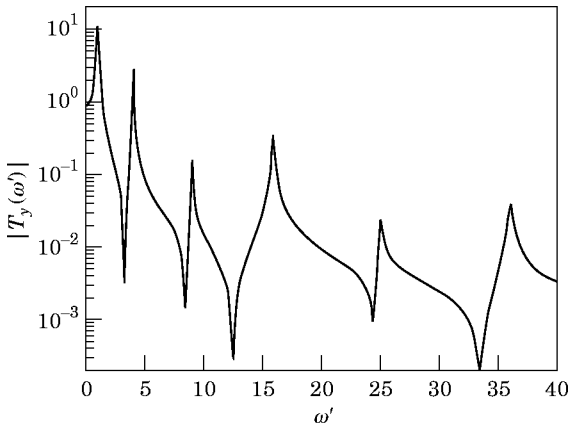

Figure 6. Transfer function magnitude $|\mathbf{T}_y(\omega')|$ at the connection point to the supporting structure for example Case I.

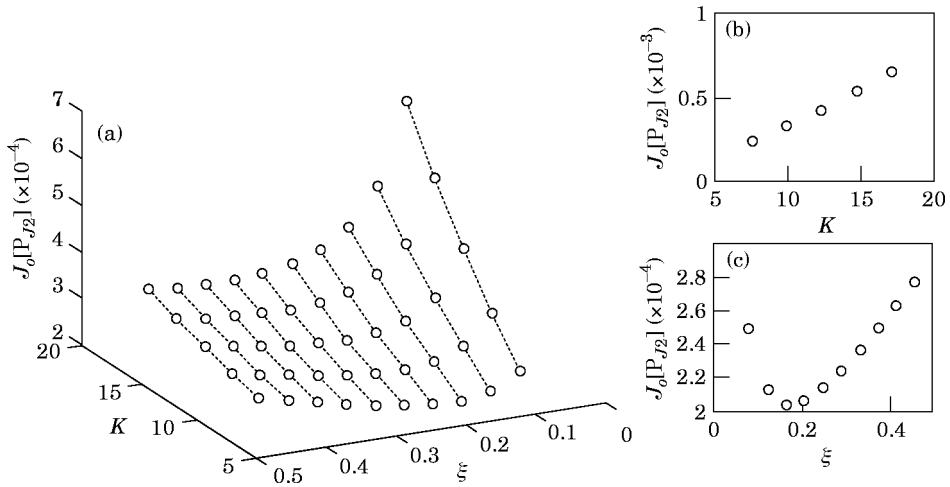

Figure 7. Optimization results for the linear passive isolator configuration of example Case I. Here, cost function J_o with respect to mount linear stiffness K and linear viscous damping ξ is shown. (a) $J_o[P_{J2}(K, \xi)]$ (——, invariant ξ); (b) $J_o[P_{J2}(K)]$, $\xi = 0{\cdot}01$; (c) $J_o[P_{J2}(\xi)]$, $K/\mu = 1$.

that the best linear stiffness value K is the lowest allowable value based on the static deflection considerations. In Figure 9, $J_o[P_{J2}]$ as a function of active parameters a_{rc} and a_{ic} is shown for $\xi = 0{\cdot}3128$ and $K/\mu = 1$. Vibratory power transmission $P_{J2}(\omega)$ as a function of excitation frequency ω for optimal linear-active cases as compared in Figure 8 to optimal linear passive cases. Addition of the active force component has significantly improved the mount performance.

Next, one considers the non-linear passive mount with cubic stiffness coefficient κ. Again, it is observed that the optimal stiffness value is the one which exactly satisfies the static deflection criteria of equation (18). In Figure 10, $J_o[P_{J2}]$ as a function of ξ and equation (18) is shown. Here, note that a softening cubic stiffness value, $\kappa < 0$, seems to improve system performance. This intuitively makes sense since the mount dynamic

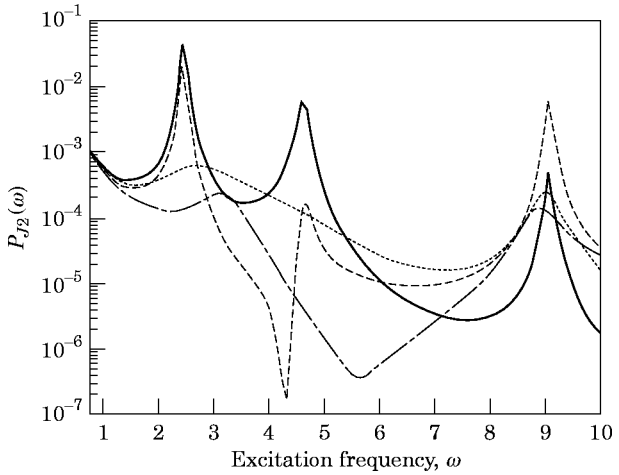

Figure 8. Transmtted power spectra, $P_{J2}(\omega)$, for the linear isolator configurations of example Case I. Refer to Table 1 for the identification of subcases. Key: ——, Case 1a (K optimized—passive); · · ·, Case 1b (K and ξ optimized—passive); – – –, Case 1c (K, a_{rc}, and a_{ic} optimized—active); —·—, Case 1d (k, ξ, a_{rc}, and a_{ic} optimized—active).

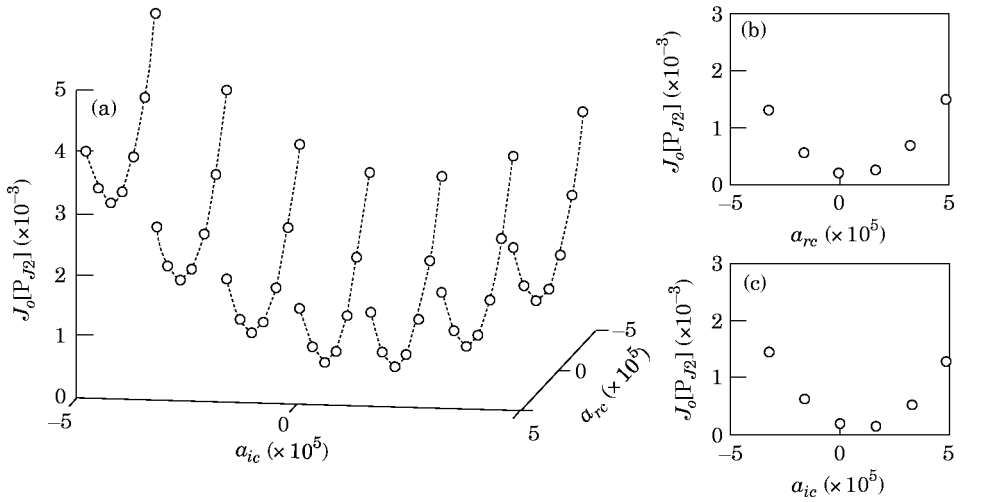

Figure 9. Optimization results for the linear-active isolator configuration of example Case I. Here, cost function J_o with respect to mount active forces a_{rc} and a_{ic} for $K/\mu = 1$ and $\xi = 0{\cdot}3128$ is shown. (a) $J_o[P_{J2}(a_{cr}, a_{ic})]$ (——, *invariant* a_{ic}); (b) $J_o[P_{J2}(a_{rc})]$, $a_{ic} = 0$; (c) $J_o[P_{J2}(a_{ic})]$, $a_{rc} = 0$.

stiffness is effectively lowered without affecting its static stiffness value. The computational optimization strategy verifies this finding. The vibratory power transmission $P_{J2}(\omega)$ as a function of excitation frequency ω for the optimal non-linear passive case is compared in Figure 11 to optimal linear passive cases. Addition of a specific non-linearity has significantly improved mount performance. Use of a very strong non-linearity results in a failure of the iterative computational procedure to converge to a solution, suggesting that as the strength of this particular non-linearity is increased, at some point a steady state periodic system response does not exist.

Finally, a non-linear active mount is considered where all five design parameters are simultaneously optimized using the Galerkin-based strategy. Again, it is found that the

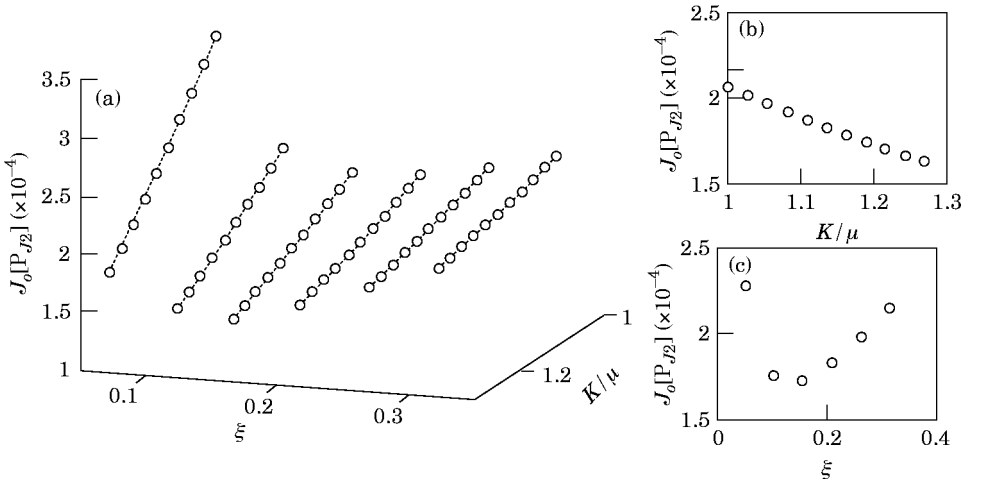

Figure 10. Optimization results for the nonlinear-passive isolator configuration of example Case I. Here, cost function J_o with respect to mount non-linear stiffness κ and linear viscous damping ξ is shown [K is adjusted to satisfy static deflection constraint—equation (18)]. (a) $J_o[P_{J2}(\kappa, \xi)]$ (——, *invariant* ξ); (b) $J_o[P_{J2}(\kappa)]$, $\xi = 0{\cdot}209$; (c) $J_o[P_{J2}(\xi)]$, $K/\mu = 1{\cdot}136$.

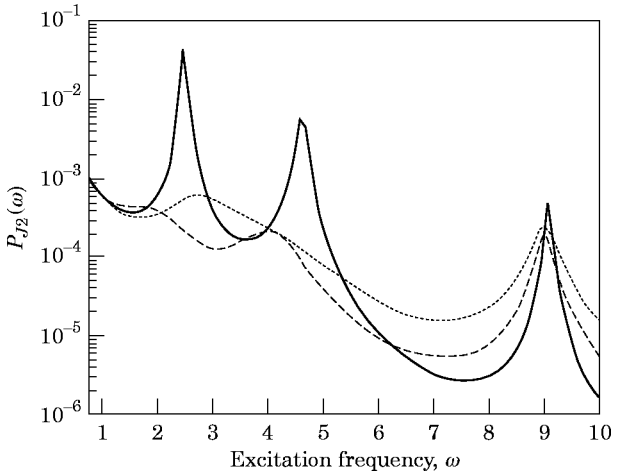

Figure 11. Transmitted power spectra, $P_{J2}(\omega)$, for the passive isolator configurations of example Case I. Refer to Table 1 for the identification of subcases. Key: ——, Case 1a (K optimized—linear); · · ·, Case 1b (K and ξ optimized—linear); – – –, Case 1e (K, ξ, and κ optimized—non-linear).

optimal stiffness value is the one which exactly satisfies the static deflection criteria of equation (18). In Figure 12, vibratory power transmission $P_{J2}(\omega)$ as a function of excitation frequency ω for the optimal non-linear active case is compared to optimal linear active cases. Addition of the active component has significantly improved mount performance. Addition of the stiffness non-linearity to this active system has resulted in a marginal improvement. Again, an upper limit on the strength of the nonlinearity has been reached for which a steady state periodic solution can be found.

The results of the six example configurations of Table 1 are summarized in Figure 13. Here it is seen that improved mount performance can be achieved via adjustment of passive linear, passive non-linear, and active mount components. However, simultaneous adjustments in combinations of these parameters could yield even greater improvement in performance. Modifications to the mount affect both the input power by changing the

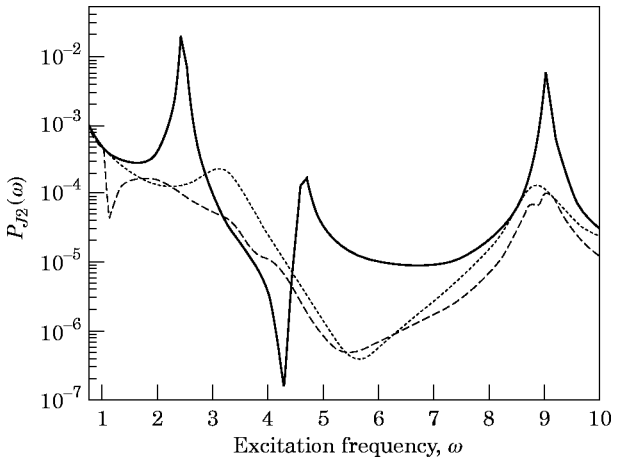

Figure 12. Transmitted power spectra, $P_{J2}(\omega)$, for the active isolator configurations of example Case I. Refer to Table 1 for the identification of subcases. Key: ——, Case 1c (K, a_{rc}, and a_{ic} optimized—linear); · · ·, Case 1d (K, ξ, a_{rc}, and a_{ic} optimized—linear); – – –, Case 1f (K, ξ, κ, a_{rc}, and a_{ic} optimized—non-linear).

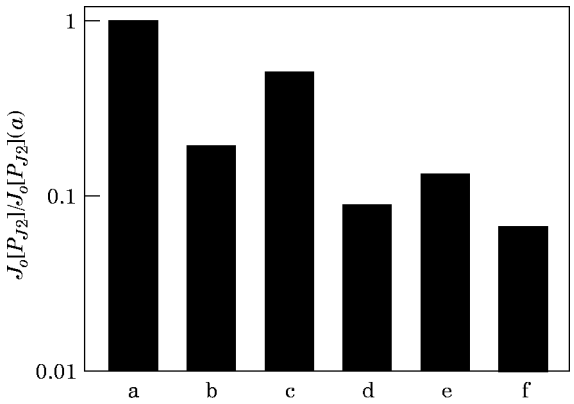

Figure 13. Summary of vibratory power flow results for example Case I. Refer to Table 1 for the identification of sub-cases.

impedance condition at the drive point and the transmitted power. In non-linear cases, it is seen that addition of a softening cubic stiffness enhances mount performance in both passive and active cases, without increasing the static deflection. An additional issue that should be considered in an assessment of performance is the secondary energy source expenditure curtailed in the active strategies. For this example case, use of the alternate performance criteria of transmitted force, equation (17), resulted in similar, although not identical, optimal mount conditions. Further study including a critical comparison of alternate performance indices is needed; it is beyond the scope of this article.

6. EXAMPLE CASE II: EXPERIMENTAL STUDY OF A NON-LINEAR VIBRATION ISOLATOR

6.1. SYSTEM MODEL

The physical system considered without the active force element is experimentally analyzed in some detail by the same authors in a companion article [16]. Important features affecting the mount optimization are summarized here. A diagram of this system is shown in Figure 14. Because of finite beam flexure and moment coupling between the beam, the mount, and the rigid mass, vertical system excitation results in horizontal and rotational motions at the mount and rigid mass in the plane of the system diagram of Figure 14. An accurate multi-dimensional system model cannot be developed easily because of the difficulty in measuring rotational mount stiffness and damping parameters. Hence, for this study, the simplified vertical motion model is used for analysis in only those frequency regimes that are not significantly affected by rotational and horizontal motions. It is modeled in much the same way as the isolation system of Section 5 (Figure 5) with the addition of a small mass m_y representing the mount footing on the beam. Also, the vertical force across the mount is approximated with a hardening stiffness polynomial (with terms up to the fifth order), a linear viscous damping component, and an active control force of the form

$$F_y(t) = K[1 + \kappa_{e1}(x(t) - y(t)) + \kappa_{e2}(x(t) - y(t))^2 + \kappa_{e3}(x(t) - y(t))^3 + \kappa_{e4}(x(t) - y(t))^4](x(t) - y(t)) + 2\xi\sqrt{MK}(\dot{x}(t) - \dot{y}(t)) + F_{AC}(t). \quad (19)$$

Pertinent system parameter values for the simplified vertical motion model are provided in Table 2.

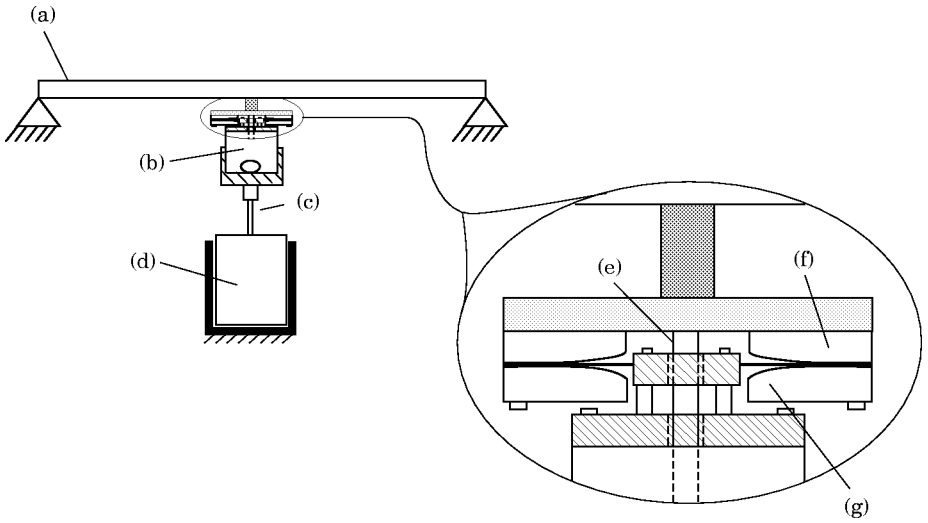

Figure 14. Schematic of the experimental setup (example Case II). (a) Simply supported beam, (b) rigid body (electrodynamic shaker with rigid harness), (c) external force input, (d) excitation (electrodynamic shaker), (e) active force input, (f) non-linear stiffness hardening element, (g) curvature exaggerated. Refer to reference [16] for more details.

6.2. MEASUREMENT ISSUES

The experimental test system was driven by harmonic excitation that was swept up and down at a rate of 0·5 Hz/s. Decreasing the sweep rate further did not alter the response; i.e., steady state was still achieved. An eight channel Hewlett Packard 3566a Dynamic Signal Analyzer and an array of force transducers and accelerometers were used

TABLE 2

Summary of experimental example (Case II) results

a: Selected parameter values (see reference [16] for a more complete list)

$K = 2{\cdot}74 \times 10^5$ N/m	$\kappa_{e3} = 6{\cdot}04 \times 10^{13}$ m^{-3}	$m = 1$	$s_b/l_s = 3/8$
$\kappa_{e1} = 3{\cdot}62 \times 10^4$ m^{-1}	$\kappa_{e4} = 2{\cdot}29 \times 10^{17}$ m^{-4}	$n = 15$	$\xi = 0{\cdot}01$
$\kappa_{e2} = 4{\cdot}48 \times 10^9$ m^{-2}	$M = 3{\cdot}307$ kg	$N_w = 6$	

b: Results

	passive case		active case	
Power Quantity* (mW)	experiment (Fig. 15)	theory	experiment (Fig. 16)	theory
Power input (P_{f1})				
primary harmonic	50·9	43·7	30·2	−2·52
super-harmonics	−0·1	0	−0·3	0
Total	**50·8**	**43·7**	**29·9**	**−2·52**
Active Power input (P_{AC})				
primary harmonic	0	0	−2·07	12·5
super-harmonics	0	0	3·27	0
Total	**0**	**0**	**1·20**	**12·5**
Power transmitted ($P_{J2(V)}$)				
primary harmonic	7·47	6·61	4·80	4·35
super-harmonics	2·73	3·69	1·45	0·22
Total	**10·2**	**10·3**	**6·25**	**4·57**

*Averaged over $150 < \omega/2\pi < 200$ Hz.

to record the system response; refer to reference [16] for a complete list of instrumentation. Impedance heads provided direct measurements of vertical excitation force $U(t)$ and response acceleration $\ddot{x}(t)$ at the excitation input point and vertical response force $F_y(t)$ and acceleration $\ddot{y}(t)$ at the interface between the mount and supporting structure. Additional transducers provided measurement of the horizontal motion of the system, the beam response, and the active force input.

Measurement of periodic system response to harmonic excitation, including sub and superharmonic components can be made with the signal analyzer by using its order tracking function. Up to five sub and/or superharmonics of the measured signals can be tracked as a function of excitation frequency ω. Cross and auto-spectra of the measured system signals at each selected harmonic of ω are estimated by the analyzer with the phase linked to the excitation force signal. Here, the auto- and cross-spectra of a signal q for the jth order harmonic of the kth order subharmonic are denoted as $\mathrm{Au}[\tilde{q}(j\omega/k)] \equiv \tilde{q}(j\omega/k)^* \ \tilde{q}(j\omega/k)$ and $\mathrm{Cr}[\tilde{q}(j\omega/k)] \equiv \tilde{q}(j\omega/k)]^*\tilde{U}(j\omega/k)$ where superscripts $\sim$ and $*$ denote a complex value and a complex conjugate, respectively. From these values, the amplitude of the response of q can be estimated as a function of ω at any sub or superharmonic. Phase information for q at a particular harmonic relative to the phase of the excitation force at that particular harmonic is also available.

In this manner, the dynamic response of force and displacement variables of the experimental system under consideration was analyzed; it is described in detail in another paper [16]. In this article, vibratory power transmission is the focus of our interest. Expressions can be formulated for estimating the vibratory power input to the system from the disturbance source P_{i1} and from the active control source P_{iJ} and the vertical-translational vibratory power transmission into the support base $P_{J2(V)}$ including, for example, the first five superharmonics of the fundamental excitation frequency:

$$P_{i1}(\omega) = \sum_{j=1}^{5} \mathrm{Re}\left[\frac{i}{2j\omega}\,(\mathrm{Cr}[\ddot{x}\tilde{(}\,j\omega))^*\right], \tag{20a}$$

$$P_{iJ}(\omega) = \sum_{j=1}^{5} \mathrm{Re}\left[\frac{i}{2j\omega}\,\frac{(\mathrm{Cr}[\ddot{y}\tilde{(}\,j\omega)] - \mathrm{Cr}[\ddot{x}\tilde{(}\,j\omega)])^*\mathrm{Cr}\,[\tilde{F}_{AC}(\,j\omega)]}{\mathrm{Au}\,[\tilde{U}(\,j\omega)]}\right], \tag{20b}$$

$$P_{J2(V)}(\omega) = \sum_{j=1}^{5} \mathrm{Re}\left[\frac{i}{2j\omega}\,\frac{\mathrm{Cr}\,[\ddot{y}\tilde{(}\,j\omega)]^*\mathrm{Cr}\,[\tilde{F}_y(\,j\omega)]}{\mathrm{Au}[\tilde{U}(\ j\omega)]}\right]. \tag{20c}$$

An inherent assumption of equations (20a–c) is that the primary (disturbance) and secondary (control) force inputs, $U(t)$ and $F_{AC}(t)$ respectively, are purely vertical-translational. Any horizontal-translational or rotational forces transmitted through the shakers stingers have been neglected. Also, in equation (20b), it is assumed that any phase mismatch between the accelerometers measuring $\ddot{x}$ and $\ddot{y}$ is negligible. Note that here it has *not* been assumed that the force inputs are harmonic, as in the computational example case in Section 5, even though the excitation signal into the amplifier for the disturbance shaker is harmonic and the reference signal for the feedforward control force is, in fact, $U(t)$.

6.3. RESULTS

Estimates of vibratory power input and transmission were made based on equation (20) and experimental order tracking data. First, in Figure 15, for the passive system one can see the vibratory power input and transmission through the vertical-translational degree-of-freedom of the mount at the first, second, third and fifth harmonics of the

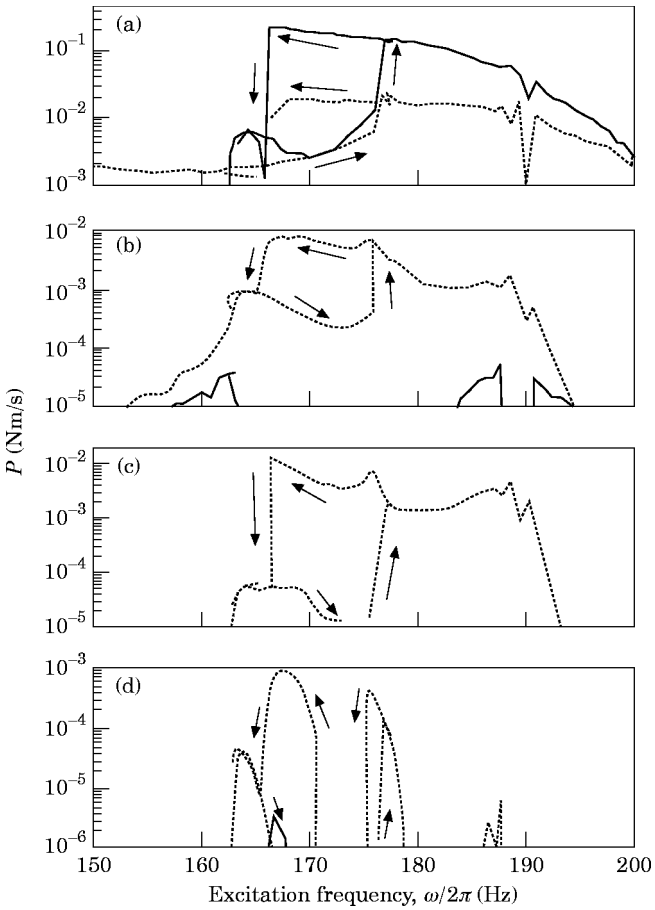

Figure 15. Results for the passive configuration of example Case II. Vibratory power transmission spectra at selected harmonics based on order tracking measurements are shown. Arrows indicate the excitation sweep direction. Key: ——, vibratory power input, P_{I1}; · · ·, vibratory power transmission, $P_{J2(V)}$; (a) first harmonic, (b) second harmonic, (c) third harmonic, (d) fifth harmonic.

excitation frequency. The power transmission $P_{J2(V)}$ is negligible at subharmonics and continues to taper off at higher superharmonics. Note that while the vibratory power input P_{I1} at harmonics other than the fundamental is minimal, it is finite due to source dynamics.

The strong softening resonance in this excitation frequency range is primarily due to an out-of-phase motion between the mounted mass M and the beam vibrating in its second mode of deformation. Vertical mass motion is accompanied by minor horizontal and rotational motion as well. Additionally, due to the stiffness non-linearity, system resonances at integer harmonics of the excitation frequency are simultaneously excited to varying degrees throughout the range. As a result, a greater amount of vibratory power is transmitted into the base than is inputed to the system at the superharmonics. Clearly, in this case, consideration of vibratory power transmission only at the fundamental harmonic would give an erroneous account of the total transmitted power.

Spectrally averaged calculations of the experimental vibratory power transmission are provided in Table 2 along with calculations made using a computational model of the system. Predictions match with measurements only in a qualitative sense but they support

the conclusion that system non-linearity results in significant vibratory power transmission at higher harmonics of the excitation frequency.

Next, the system response in the presence of an active mount force in parallel with the nonlinear stiffness element, as shown in Figure 14, is considered. The active force signal is produced using a Digisonix dx-57 digital sound and vibration controller [25]. This device uses a feed-forward adaptive control algorithm, requiring a reference signal and an error signal to enable adaptation of the control filter coefficients for optimal performance. The excitation force input $U(t)$ to the rigid body was used as the reference signal, and the vertical-translational force transmitted to the simply supported beam $F_y(t)$ was used as the error signal. Low level broad band random excitation over the frequency range of interest was used to optimally adapt the filter coefficients. Swept sine excitation resulted in instability of the adaptive algorithm near resonances where multiple solution paths existed. Hence, before switching from broad band excitation to swept sine excitation, the filter coefficient adaptation process had to be halted. Since the algorithm design of active control is not the focus of this paper, further details of the implemented algorithm are not discussed. Instead, the focus is on the resulting system response for a particular active force input.

Vibratory power content at the first, second, third, and fifth harmonics of the excitation frequency is shown in Figure 16. Results from this case are also summarized in Table 2. Addition of an active component has attenuated power transmission into the supporting structure. This is accomplished primarily by altering the impedance condition at the excitation input point, thereby reducing P_{i1}. It is interesting to note that the active force component does provide a substantial power input at higher harmonics of the excitation frequency. Studies indicated that the active control source does not provide an ideal harmonic force at the reference signal frequency, but rather has its own dynamics and represents a complex impedance connection to the non-linear system. System response at higher harmonics is dynamically coupled to the control source dynamics.

Results of the computational study are also summarized in Table 2. In this case, a good match with experimental data is unattainable. While a measurement of the excitation frequency-dependent magnitude and phase of the primary harmonic of the active force input with respect to the disturbance force input was available, only the magnitude of higher harmonics of the active force input could be extracted from the order tracking data. Consequently, in the computer simulation, the active force is described only at the fundamental harmonic component. Nonetheless, trends similar to those measured are predicted by the computational model. For instance, vibratory power transmission into the support structure, P_{J2}, is reduced, as is vibratory power input from the disturbance source, P_{i1}, in this case to a negative value.

7. CONCLUSION

In this paper, an analytical framework for the design optimization of a somewhat realistic multi-degree-of-freedom mounting system has been formulated. Non-linear effects in the mount, and parallel passive design and active control concepts have been accounted for in an overall strategy that uses vibratory power flow to assess the dynamic performance of a vibration mount. The proposed scheme has been applied to the optimization of a generic isolation system, illustrating the utility of using both non-linear and active control concepts concurrently to improve performance over traditional linear passive mount designs.

Study of an experimental isolation system has led to a better understanding of vibratory power transmission in both passive and active non-linear systems. Multi-frequency

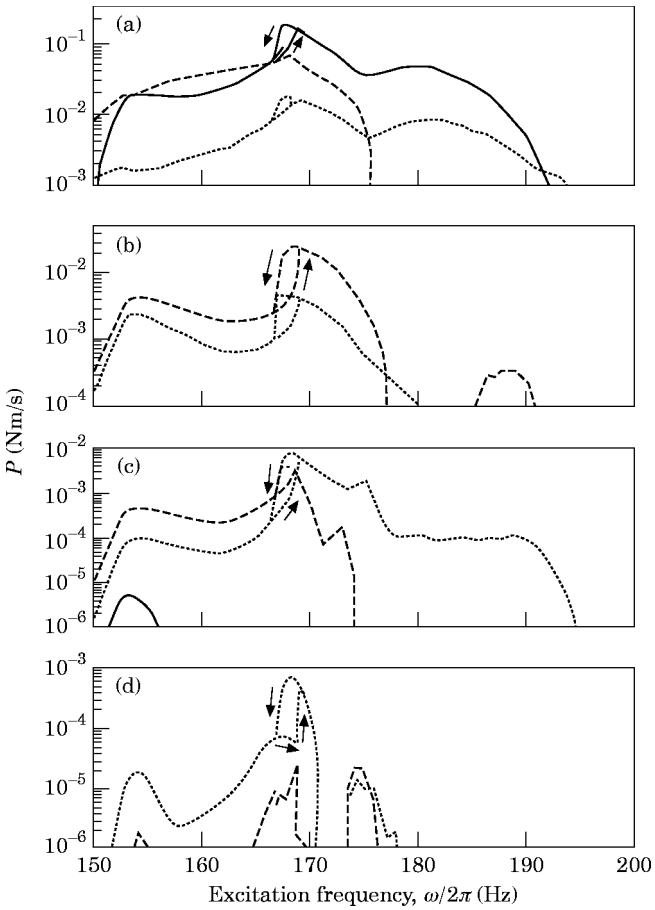

Figure 16. Results for the active configuration of example Case II. Vibratory power transmission spectra at selected harmonics based on order tracking measurements are shown. Arrows indicate the excitation sweep direction. Key: ——, vibratory power input, P_{i1} (from disturbance); · · ·, vibratory power transmission, $P_{J2(V)}$; ——, vibratory power input, P_{iJ} (from active source); (a) first harmonic, (b) second harmonic, (c) third harmonic, (d) fifth harmonic.

vibratory power transmission involving numerous system resonances can result from single-frequency vibratory power input. This multi-harmonic response to harmonic excitation in combination with non-ideal active source dynamics may result in the active component having an unanticipated influence on system behavior at these other frequencies. Additionally, it has been shown that the existence of multiple solution paths under identical excitation conditions can render conventional feed-forward active control approaches with adaptive algorithms unstable. Obviously, further study is needed to clarify these and other relevant research issues; this work is in progress.

ACKNOWLEDGMENTS

The authors wish to acknowledge the Office of Naval Research Graduate Fellowship Program, the Center for Automotive Research at the Ohio State University, the U.S. Army Research Office URI Grant DAAL-03-92-G-0120 and the ASSERT Project; (project monitor: Dr. T. L. Doligalski) and the Ohio State University Graduate School for their

financial support. Dr. C. Padmanabhan and Dr. T. E. Rook are also acknowledged for helpful advice and insight into nonlinear systems and computational methods.

REFERENCES

1. J. P. Den Hartog 1985 *Mechanical Vibrations*. Mineola, NY: Dover; reprint of 4th edition.
2. G. Kim and R. Singh 1995 *Journal of Sound and Vibration* **179**, 427–453. Study of passive and adaptive hydraulic engine mount systems with emphasis on non-linear characteristics.
3. P. L. Graf and R. Shoureshi 1988 *ASME Journal of Dynamic Systems, Measurement, and Control* **110**, 422–429. Modeling and implementation of semi-active hydraulic engine mounts.
4. G. Kim and R. Singh 1994 *Society of Automotive Engineers Paper no*. 932897. Engine vibration control using passive, active and adaptive hydraulic mount systems.
5. N. Vahdati and J. A. Pike 1993 *Second Conference on Recent Advances in Active Control of Sound and Vibration* 459–481. Analytical comparison of active versus passive aircraft engine suspensions.
6. W. A. Welsh, P. C. Von Hardenberg, P. W. Von Hardenberg and A. E. Staple 1990. *46th Annual Forum Proceedings of the American Helicopter Society*, 21–37. Test and evaluation of fuselage vibration utilizing active control of structural response (ACSR) optimized to ADS-27.
7. C. W. Bert, D. E. Egle and D. J. Wilkins, Jr. 1990 *Journal of Sound and Vibration* **137**, 347–352. Optimal design of a non-linear dynamic absorber.
8. I. N. Jordanov and B. I. Cheshenkov 1988 *Journal of Sound and Vibration* **123**, 157–70. Optimal design of linear and non-linear dynamic vibration absorbers.
9. W. J. Carter and F. C. Liu 1961 *ASME Journal of Applied Mechanics* **28**, 67–70. Steady-state behavior of non-linear dynamic vibration absorber.
10. A. Soom and M-S. Lee 1983 *ASME Journal of Vibration, Acoustics, Stress, and Reliability in Design* **105**, 112–119. Optimal design of linear and non-linear vibration absorbers for damped systems.
11. S. Natsiavas 1992 *Journal of Sound and Vibration* **137**, 347–352. Steady state oscillations and stability of non-linear dynamic vibration absorbers.
12. B. Ravindra and A. K. Mallik 1993 *Journal of Sound and Vibration* **170**, 325–337. Performance of non-linear vibration isolators under harmonic excitation.
13. C. L. Kirk 1988 *Journal of Sound and Vibration* **124**, 157–182. Non-linear random vibration isolators.
14. H. Kojima and H. Saito 1983 *Journal of Sound and Vibration* **88**, 559–68. Forced vibrations of a beam with a non-linear dynamic vibration absorber.
15. T. J. Royston and R. Singh 1996 *Journal of Sound and Vibration* **194,** 243–263. Periodic response of mechanical systems with local nonlinearities using an enhanced Galerkin technique.
16. T. J. Royston and R. Singh 1996 *Journal of Sound and Vibration* (to appear). Experimental study of a mechanical system containing a local continuous stiffness non-linearity under periodic excitation and a static load.
17. H. Ashrafiuon and C. Nataraj 1991 *ASME Journal of Vibration and Acoustics* **34**, 191–196. Dynamic analysis of engine mount systems.
18. R. J. Pinnington and R. G. White 1981 *Journal of Sound and Vibration* **75**, 179–197. Power flow through machine isolators to resonant and non-resonant beams.
19. J. Farstad and R. Singh 1995 *Journal of the Acoustical Society of America* **97**, 2855–2865. Structurally transmitted dynamic power in discretely joined damped component assemblies.
20. M. D. Jenkins, P. A. Nelson, R. J. Pinnington and S. J. Elliott 1993 *Journal of Sound and Vibration* **166**, 117–140. Active isolation of periodic machinery vibrations.
21. K. B. Scribner, L. A. Sievers and A. H. Von Flotow 1993 *Journal of Sound and Vibration* **167**, 17–40. Active narrow-band vibration isolation of machinery noise from resonant substructures.
22. J. Pan, C. H. Hansen and J. Pan 1993 *Journal of the Acoustical Society of America* **94**, 1425–1434. Active isolation of a vibration source from a thin beam using a single active mount.
23. J. Pan and C. H. Hansen 1993 *Journal of the Acoustical Society of America* **93**, 1947–1953. Active control of power flow from a vibrating rigid body to a flexible panel through two active isolators.
24. K. F. Graff 1975 *Wave Motion in Elastic Solids*. New York: McGraw-Hill.
25. *Digisonix Commercial and Industrial Systems* 1992. dx-57 Digital Sound and Vibration Controller Installation, Operation, and Maintenance Manual, Digisonix Division, Nelson Industries, Inc.

APPENDIX A: LIST OF SYMBOLS

A	cross-sectional area of beam
Au	Auto spectrum
$\mathbf{a}_k^{\mathbf{F_q}}$	kth coefficient in Fourier series representation of $\mathbf{F}_q^{mn}$
$\mathbf{a}_k^{\mathbf{q}}$	kth coefficient in Fourier series representation of $\mathbf{q}^{mn}$
a_{rc}, a_{ic}	in-phase and out-of-phase components of the active control force
a^U	harmonic excitation amplitude
Cr	cross-spectrum
$\mathbf{D}_j^{\mathbf{q}}$	qth Fourier coefficient of $\mathbf{d}^{\mathbf{q}}$
d.o.f.	degree of freedom
$\mathbf{d}^{\mathbf{q}}$	vector of Galerkin determining equations for q
E	Young's modulus of beam
F_{AC}	active control force input
$\mathbf{F}_q^{mn}$	force vector for system solution with m subharmonics and n superharmonics
g	gravitational constant
I	moment of inertia of beam
Im	imaginary part
i	$\sqrt{-1}$
$\mathbf{J}$	Jacobian of Galerkin determining equations – in the frequency domain
J_0	scalar cost function of mount optimization procedure
K	linear stiffness coefficient of mount
M	rigid body mass
m	number of sub-harmonics assumed in the nonlinear solution
m_b	modal mass for simply supported beam
n	number of superharmonics assumed in the nonlinear solution
N_q	dimension of qth displacement/force vector or number of d.o.f. in qth component or subsystem
P_{ij}	vibratory power transmission between the ith and jth subsystems
$\mathbf{Q}$	subspace of allowable values for Γ
$\mathbf{q}^{mn}$	displacement vector for system solution with m subharmonics and n superharmonics
R	residual to be minimized in iterative Galerkin procedure
Re	real part
s	axial position on beam
s_b	axial position of mount connection point to beam
t	time
$\mathbf{T}_q$	transfer function matrix of qth displacement/force vector pair
U	dynamic excitation force
u	vertical displacement of beam
$\mathbf{w}$	vector of displacement variables in Section (B)
$\mathbf{x}$	vector of displacement variables in Section (A)
$\mathbf{y}$	vector of displacement variables connecting Section (B) to Section (A)
$\boldsymbol{\alpha}^{\mathbf{q}}$	matrix of Fourier series coefficients of Galerkin solution for qth displacement vector
Γ	vector of mount design parameters
δ	Dirac delta function
ξ	mount linear damping coefficient
ζ_j	beam modal damping ratio
κ	non-linear stiffness coefficient of mount (subscript e denotes experimental case)
l_s	axial length of beam
ρ	material density of beam
τ	non-dimensional time
ω	excitation frequency (rad/s)
ω'	response frequency (rad/s)
ω_j	natural frequency of jth mode of the simply supported beam ($\omega_b = \omega_1$)
Ω	system or excitation parameter

Superscripts

$*$	complex conjugate
$\sim$	complex variable